Electrochimica Acta 215 (2016) 289–297

Contents lists available at ScienceDirect

Electrochimica Acta

journal homepage: www.elsevier.com/locate/electacta

Impact of molecular structure of two natural phenolic isomers on the protective characteristics of electropolymerized nanolayers formed on copper

Marcos Bertuola[a], Diego E. Pissinis[a], Aldo A. Rubert[a], Eduardo D. Prieto[a], Mónica A. Fernández Lorenzo de Mele[a,b,*]

[a] Instituto de Investigaciones Fisicoquímicas Teóricas y Aplicadas (INIFTA), CONICET, Facultad de Ciencias Exactas, Departamento de Química, Universidad Nacional de La Plata, Casilla de Correo 16, Sucursal 4, 1900 La Plata, Argentina
[b] Facultad de Ingeniería, Universidad Nacional de La Plata, Calle 47 y 1, 1900 La Plata, Argentina

ARTICLE INFO

Article history:
Received 25 April 2016
Received in revised form 16 August 2016
Accepted 20 August 2016
Available online 21 August 2016

Keywords:
carvacrol
thymol
copper
nanolayer
electropolymerization

ABSTRACT

A comparative study of the electropolymerization of two natural phenolic isomers, carvacrol (Carv) and thymol (TOH) on copper was made. They are components of *Origanum vulgare* and *Thymus vulgaris* essential oils. Polymerized layers (polyCarv and polyTOH) were attained by cyclic voltammetry (CV). Electrochemical techniques complemented by ATR-FTIR, XPS, SEM and AFM surface analyses were used to evaluate the composition and protective characteristics of the films. Results revealed that the electrochemical response in chloride solutions was dissimilar. Copper ions release by polyCarv in chloride solutions was lower than 30% of that obtained with TOH treatments. PolyCarv is a highly protective, transparent film, remarkably different from the brownish, rough and non-protective film obtained with TOH. ATR-FTIR results showed that the oxidation of adsorbed Carv and TOH led to cetonic structures while after electropolymerization ether bonds were also found. However, polyCarv and polyTOH showed important differences in ν-OH band. Deconvolution of C1s signal of XPS spectra led to four contributions with different proportions for polyCarv and polyTOH. Accordingly, $C_{(ph)}$-O is 50% of total C1s for polyCarv and 30% for polyTOH. C1s/O1s relationships were also different. AFM and SEM observations showed the presence of round flakes, smaller for polyCarv (5 nm height) than for TOH (35 nm height). A compact layer was found in case of polyCarv but cauliflower and sticks structures with cracks were found for polyTOH. In summary, results showed the important impact of the molecular structure on the composition, structure and protective characteristics of the polymeric layers. A mechanism is proposed to interpret these results.

1. Introduction

Copper and copper-based alloys are materials suitable for versatile purposes. They are used in construction for outdoor applications due to their attractive appearance and advantageous mechanical, thermal and conductivity properties together with their simple fabrication and joining. For industrial purposes they are extensively applied in piping, tubing, condensers and heat exchangers because of their adequate resistance to corrosion and biofouling. They have also been proposed for containers for nuclear wastes buried and exposed to ground-waters [1]. Other advantages are their reduced maintenance costs, prolonged service life, increased reliability and high recyclability [1–3].

In spite of its valuable properties copper is vulnerable against corrosion in chloride environments [4]. Apart from the economical costs involved in substitution or repair of the copper-containing system, corrosion process leads to the release of copper ions that contaminate aqueous environments and represents a potential risk for biological systems [5]. Chloride ions adsorb on copper and CuCl is formed which may lead to soluble $CuCl_2^-$ complex or hydrolyze to form atacamite ($Cu_2(OH)_3Cl$) [4].

Several kinds of coatings have been proposed to reduce corrosion when metals are susceptible to environmental

* Corresponding author at: Instituto de Investigaciones Fisicoquímicas Teóricas y Aplicadas (INIFTA), CONICET, Facultad de Ciencias Exactas, Departamento de Química, Universidad Nacional de La Plata, Casilla de Correo 16, Sucursal 4, La Plata 1900, Argentina.
E-mail addresses: fernandezlorenzom@hotmail.com, mmele@inifta.unlp.edu.ar (M.A. Fernández Lorenzo de Mele).

http://dx.doi.org/10.1016/j.electacta.2016.08.100
0013-4686/

interactions [6]. Coating may act as ionic filter able to mitigate current transfer between anodic and cathodic areas, or obstruct the diffusion of oxygen to inhibit cathodic reaction. Several organic inhibitors form thin films of adsorbed molecules that cover copper active sites hindering the adsorption of chlorides and the formation of corrosion products. Many of them are hetero-cycles that are added to the corrosive solutions [7–11]. Several Inhibitory treatments were also developed with the aim of improving the shielding action achieved with adsorptive films. However, due to the more strict environmental regulations that have been implemented in recent years, corrosion inhibitors are required to have an environmentally friendly profile. They are expected to be non bioaccumulative, biodegradable and have a low toxicity level. Thus, current research is focused to the exploration of environmentally compatible, nonpolluting corrosion inhibitors. This search leads to natural factories like plants, rich sources of phytocompounds that can readily satisfy these requirements. Natural compounds are frequently low-cost, ecocompatible, renewable and readily available. Importantly, they can be extracted inexpensive by simple procedures. Consequently, substantial effort has been made in recent years to investigate the corrosion inhibiting efficacy of these natural products with low or "zero" environmental impact [12–18]. It is well known that aromatic plants like *Origanum vulgare* and *Thymus vulgaris* are sources of phenolic compounds (PC). Interestingly, electrochemical studies with some synthetic PC have revealed that they can be electropolymerized on metallic surfaces and showed excellent corrosion protection [19,20]. Thus, new strategies based in electropolymerization process of natural PC with low effect in the environment may be developed. Among non synthetic compounds two of the main components of *Origanum vulgare* and *Thymus vulgaris* essential oils (carvacrol and thymol) are PC that seem to be suitable for the development of an ecofriendly treatment [21]. Considering previous reports about different substituted PC [22], we hypothesized that both carvacrol (Carv) and thymol (TOH), due to their phenolic structures, are able to form electropolymerized layers on copper surface but their shielding action against corrosion may be different. Thus, the aim of this work is to elucidate if the molecule structure of these structural isomers impacts on their electropolymerization mechanism and on the protective characteristics of the nanolayers formed on copper. Apart from the importance of the fundamental aspects of this investigation, related the electropolymerization mechanisms of two PC isomers, Carv and TOH, results should be very useful in relation to the selection of the species of the aromatic plants that will be the best sources of the essential oils to be used as corrosion inhibitors. For example, they will provide information to select the best species between, *Origanum vulgare*, reach in Carv and *Origanum X applii or Thymus vulgaris* whose main component is TOH [23–25].

2. Experimental

2.1. Chemicals

Carv (Sigma, St. Louis, MO, USA), and TOH (Sigma, St. Louis, MO, USA) which chemical structures are shown in Fig. 1 were used in the experiments. All chemicals consumed in the assays were of analytical grade and ultrapure water was employed to prepare the solutions.

2.2. Cu samples and generation of electropolymerized layers.

Cylindrical copper bars (99.7% electrolytic metal copper, 0.9 cm diameter) (Merck, Darmstadt, Germany), whose lateral surfaces were covered with polyoxymethylene, leaving an exposed area of

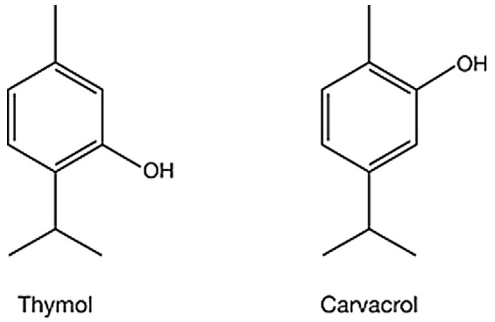

Fig. 1. Chemical structure of thymol and carvacrol.

0.626 cm^2 were used as working electrodes for electrochemical experiments. Each electrode was mechanically polished with emery paper of different grain sizes using water as lubricant and then washed with water and ethanol, and dried with nitrogen. The electrode surface was carefully observed under optical microscope (Olympus BX51, Olympus Corp., Tokyo, Japan), before and after the experiments, to evaluate possible changes in color and/or texture of copper.

Electrochemical assays were made in a conventional cell with double wall to allow the circulation of water at constant temperature. A platinum foil was used as counter electrode and a saturated calomel electrode (SCE) as reference electrode. The potential values in the text are referred to the SCE.

Electropolymerized films of Carv and TOH (polyCarv and polyTOH) were attained using cyclic voltammetry (CV) by successive cycling the electrode potential at 50 mV s^{-1} (39 cycles) within 0.3 V–1.0 V potential range. This electrochemical methodology was a modification of that reported by Guenbour [26,27]. In our case 0.1 M Carv or 0.1 M TOH, 70:30 water/ethanol (EtOH) alkaline solution (0.3 M NaOH) [26–28] was used as electrolyte for CV electropolymerization treatment. The presence of EtOH in Carv and TOH solutions is necessary to improve PC solubility. Each test was run in triplicate to verify the reproducibility of the data. In all cases a potentiostat-galvanostat TEQ03 was used. Control experiments using 0.3 M NaOH with and without EtOH were also recorded.

For surface analysis and copper ion release measurements, copper disks obtained from a pure copper sheet (99.7%, 0.1 mm thick, 6 mm diameter) (Merck, Darmstadt, Germany) were used. These disks were washed with (5% v/v) H_2SO_4, vigorously rinsed with ultrapure water and then dried with nitrogen. The polyCarv/polyTOH formation on the disks was carried out with the copper sheets as previously described for cylindrical copper samples.

2.3. Measurement of copper ions release

The copper ion release from the copper disks covered by polyCarv or polyTOH films (polyCarvCu, polyTOHCu) after their immersion in 3 ml of KCl solution (0.136 M) for 1 day, 3 days and 6 days at room temperature was measured by colorimetric analysis and by atomic absorption spectroscopy. Colorimetric method is based on the addition of 1-(2 pyridylazo)-2-naphthol (PAN) to the samples. This dye forms colored complexes with Cu(II) which are suitable for spectrophotometric analysis. Briefly, an appropriate volume of H_2SO_4 was added to each sample to reach a final concentration of 0.25 M. An aliquot of 100 μl of these acidic samples was mixed with 100 μl of 4 mM PAN ethanolic dissolution and 800 μl of water. The absorbance was measured in a Shimadzu UV 1800 spectrometer at λ=560 nm, maximum of the absorption spectra of the copper(II)−PAN complex. The copper content in an

unknown sample was determined by comparing with a calibration curve [29].

The concentration of cupric ions was also determined by Flame atomic absorption spectrometer. Shimadzu AA-7000 (Kyoto, Japan) was used for the determination of soluble copper concentration, after total dissolution with 1 ml 0.28 M nitric acid. Hollow cathode lamps were employed as radiation sources (limit of detection = 0.02 μg ml^{-1}, obtained using internal quality control, according standard procedures).

2.4. Electrochemical tests to evaluate corrosion protection.

Open circuit potential (OCP) evolution was evaluated for bare and polyCarvCu and polyTOHCu electrodes during 3 h in KCl solution.

Potentiodynamic cycling between the OCP and 0.07 V at 50 mV s^{-1} in 0.136 M KCl was employed to evaluate the stability of the protective layer by recording 20 successive cycles.

Polarization studies were also performed to evaluate the corrosion protection of the layers in 0.136 M KCl in the potential range close to OCP (from OCP to +0.3 V) at 1 mV s^{-1} using different electrodes for each assay. Chloride ions concentration was selected taking into account the concentration of chlorides in biological media and in saline aqueous ecosystems.

2.5. Surface analysis by XPS, ATR-FTIR and AFM.

XPS measurements were performed using Al Kα source (XR50, Specs GmbH) and a hemispherical electron energy analyzed (PHOIBOS 100, Specs GmbH) operating at 40 and 10 eV pass energy. A two-point calibration of the energy scale was performed using sputtered cleaned gold (Au 4f7/2, binding energy BE = 84.00 eV) and copper (Cu 2p3/2, BE = 932.67 eV) samples. C1s at 285 eV was used as charging reference. Auger parameter was calculated and used to survey the chemical modification for surface copper species, independently of the static charge of the substrate. ATR-FTIR spectra were obtained in a Varian 660 spectrometer equipped with an attenuated total reflection (ATR) accessory (MIRacle ATR, Pike technologies) with a ZnSe prism. In all cases, each spectrum was the result of 256 scans taken with a resolution of 2 cm^{-1}.

Tapping® mode AFM (Nanoscope V; Bruker, Santa Barbara, CA) in topographic mode was used to characterize the substrates, using silicon tips (ArrowTM NCR; NanoWorld, Neuchâtel, Switzerland; spring constant, 42 N/m; resonance frequency, 285 kHz). Nanoscope 7.30 and Nanoscope Analyis 1.5 softwares were employed to obtain the images (Bruker).

Scanning electron microscopy (SEM) images of polyCarvCu and polyTOHCu were taken using an environmental scanning electron microscope FEI Quanta 200.

3. Results and Discussion

3.1. Formation of polymeric films from carvacrol and thymol

Potentiodynamic measurements were performed by successive voltamperommetric cycles carried out in different solutions. Fig. 2 shows a sudden current increase in alkaline 70:30 water/EtOH solution, with a nearly linear i/E relationship for potentials higher than 0.4 V. Fig. 1S illustrates the i/E profiles obtained during the 1st and 2nd cycles between −1.0 V and +0.3 V with the control solution (0.3 M NaOH) in the absence of EtOH. During the first cycles current values show an i/E response with a marked increase of current at potentials more anodic than 0.7 V, similar to that reported in the literature [30,31], attributed to the oxidation of copper. Thus, in agreement with previous works [26,32–34] the abrupt increase of current at 0.4 V (Fig. 2) can be attributed to the oxidation of EtOH on copper that reaches a maximum at potentials higher than 0.8 V

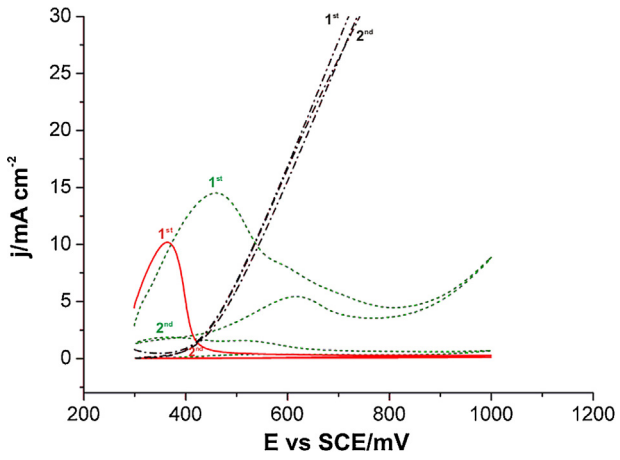

Fig. 2. First and second voltamperometric cycles made at 50 mV s^{-1} with Cu electrodes in (——) 0.1 M Carv, or (**-----**) 0.1 M TOH in 0.3 M NaOH 70/30 water/EtOH solution; (—·—·—·—) Control without PhD monomer. A control without EtOH is shown as Supplementary material (Fig. 1S).

(not shown). Fig. 2 also shows the 1st and 2nd cycles obtained with the addition of 0.1 M Carv and 0.1 M TOH. If Carv is added to the solution, an anodic peak that initiates close to 0.3 V was recorded, with current densities higher than those of the plain EtOH-containing solution at this potential. This indicates that the oxidation of Carv on Cu begins at potentials lower than that of EtOH. Subsequently, at potentials higher than 0.5 V current decreased sharply and very low currents were recorded during the return scan and the following cycles. A similar behavior was reported for phenol and phenol derivatives on different electrodes [19,35–39]. It can be inferred that the oxidation products of Carv remained on the surface and blocked the active sites hindering the oxidation of fresh EtOH and Carv from the bulk. Upon increasing the number of cycles, current decreased continuously reaching values close to 0.3 μA cm^{-2} after 39 cycles. After this treatment the electrode surface was covered by a transparent film of polyCarv.

When TOH was added to the plain EtOH-containing solution a high current peak at 0.45 V with a shoulder on the anodic side (0.6 V) were recorded (Fig. 2). They were followed by a current decrease reaching a minimum at 0.8 V with an important increase thereafter. During the cathodic scan another anodic contribution was depicted (0.6 V), indicating that oxidation activity persisted during the return scan. Even though an important current decrease was observed during the second scan, current values were higher than those recorded for Carv. Thus, during the earlier cycles, electrochemical behavior of TOH is markedly different from that of Carv. Upon increasing the number of cycles, current density decreased and after the fifth cycle current values were in the order of 400 μA cm^{-2} at 1 V (after the 39th cycle it was 110 μA cm^{-2}) notably higher than that obtained with Carv (0.3 μA cm^{-2}).

Substantial differences in the surface appearance of polyCarv and polyTOH films were noticed since a brownish layer was formed in case of polyTOH that contrasts with the transparent one developed with Carv (Fig. 3 insets). SEM images showed a homogeneous layer in case of polyCarv and a rough surface in case of polyTOH (Fig. 3). The image of polyTOH shows a ditch with sticks similar to those reported for polyphenol [39].

3.2. Electrochemical response of polymer coated copper in chloride solutions

3.2.1. Open circuit potential (OCP) records

OCP evolution was evaluated for bare and polymeric film-coated Cu electrodes during 200 min in 0.136 M KCl solution

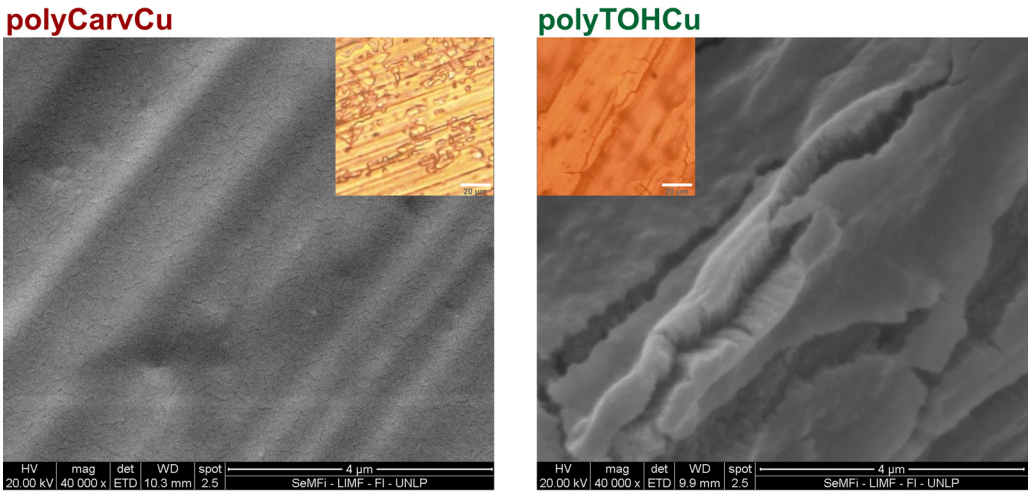

Fig. 3. SEM microphotographs showing the electropolymerized layer (CV, 39 cycles) obtained with Carv (polyCarvCu) and TOH (polyTOHCu). Insets show images obtained with optical microscopy. A brownish rough layer can be observed in case of polyTOHCu.

Table 1
Open circuit potential values (OCP) for polyCarv, polyTOH and bare copper after different periods (5 min, 80 min, 200 min).

	$OPC_{(5min)}$/mV	$OPC_{(80min)}$/mV	$OPC_{(200min)}$/mV
polyCarv	-107.6 ± 0.1	-107.6 ± 30.4	-116.1 ± 22.9
polyTOH	-112.3 ± 0.4	-109.1 ± 24.8	-111.7 ± 9.5
Bare Cu	-171.9 ± 21.1	-203.9 ± 6.8	-205.9 ± 3.2

(Table 1). The curves show a similar potential evolution but OCP values were c.a. 70 mV more anodic in case of samples with polyTOH and polyCarv layers.

3.2.2. Anodic polarization curves

In order to test the protective characteristics of polyCarv and polyTOH layers formed after CV treatments anodic polarization curves were recorded in 0.136 M KCl solution. Polarization curves for bare Cu, polyCarvCu and polyTOHCu electrodes in the potential range between OCP and +0.3 V are shown in Fig. 4. It can be observed that, at potencials >0.0 V, current densities for polyCarvCu are lower than those measured for polyTOHCu demonstrating the better shielding propierties of the polyCarv layer in chloride environments.

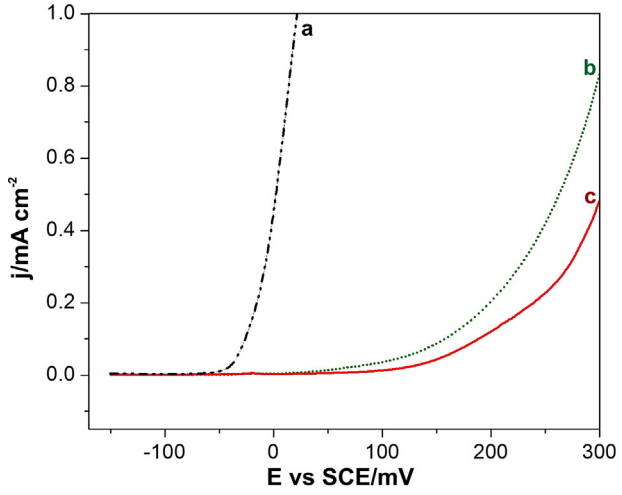

Fig. 4. Polarization curves made at 1 mV s^{-1} with copper in 0.136 M KCl without (a) and with electropolymerized layer of polyTOH (b) and polyCarv (c).

Table 2
Electrochemical current efficiency (IE%) at 100 mV, 200 mV, 300 mV (SCE) for polyCarv and polyTOH.

Electrode	$IE_{(100mV)}$/%	$IE_{(200mV)}$/%	$IE_{(300mV)}$/%
polyCarv	99.7 ± 0.2	98.6 ± 1.1	95.7 ± 1.5
polyTOH	98.4 ± 0.6	95.7 ± 1.3	89.4 ± 1.8

Table 2 shows current efficiencies (IE%) that were calculated according to:

$$IE\%\ (Ei) = \frac{i^0 - i}{i^0} \times 100$$

i^o is the current density corresponding to bare Cu and i is the current density of the polyCarvCu or polyTOHCu measured at Ei = E_{corr}, 100 mV, 200 mV or 300 mV (Table 2).

Treatments with Carv and TOH show (Table 2) high IE% values, IE% > 95% for Carv and IE% > 89% for TOH at potentials more anodic than Ecorr.

3.2.3. Cyclic potentiodynamic response of polymer coated Cu

The electrochemical response of the polyCarvCu and polyTOHCu was also tested by cycling the electrode in a potential range close to the OCP (from OCP to +0.07 V) in 0.136 M KCl

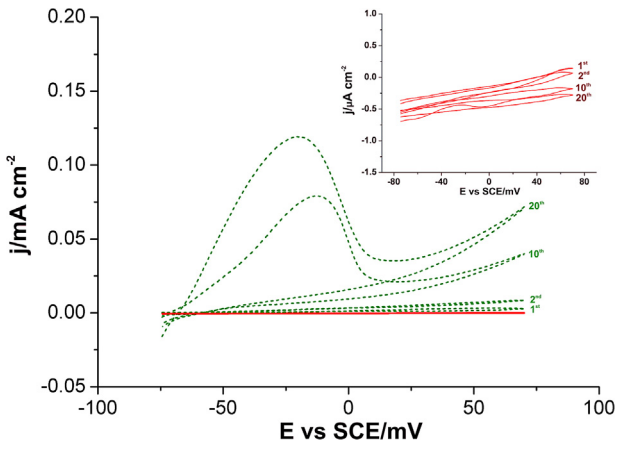

Fig. 5. Voltamperometric cycles (1st, 2nd, 10th, 20th cycles) obtained by cycling the copper electrodes between the OCP and 0.07 V at 5 mV s^{-1} in 0.136 M KCl. (___) polyCarvCu; (. . . . .) polyTOHCu. Inset: Detail of polyCarvCu curves.

solution. Fig. 5 shows that current values for polyTOH coating are initially low but upon cycling they increase and a peak is formed at −0.025 V. The shape of the curves becomes similar to that of the control obtained with the bare electrode indicating that polyTOH layer is markedly more labile than polyCarv layer. Consequently, the loose polyTOH layer progressively loses its protective characteristic in chloride solutions and oxidation of copper probably takes place on poorly sheltered sites. Conversely, the current density in case of polyCarv is lower than 1 μA cm^{-2} confirming the higher stability and inhibitory action of polyCarvCu.

3.2.4. Copper ions release in the presence and in the absence of the electropolymerized layers

Measurements of copper ions released by copper disk with and without the electropolymerization treatments in 0.136 M KCl solution (Fig. 6) are in agreement with the electrochemical behavior of polyCarvCu and polyTOHCu. They show that concentration of copper ions increases with time and after 6 days of immersion the content of copper ions reached the highest value in case of bare copper while the best protective performance was achieved by polyCarvCu. It can be noticed that treatments of 1 cycle and 39 cycles with Carv are more effective than those of TOH. The higher the number of cycles, the better the protection.

3.3. Surface analysis

3.3.1. ATR-FTIR analysis of polymer coated Cu

The infrared spectra of pure Carv, and TOH (Fig. 7) show the characteristic contributions attributed to ν-OH, bend OH and C-O structures at 3386, 1458 and 1250 cm^{-1} respectively, for Carv, and 3223, 1380 and 1244 cm^{-1} for TOH [40]. The spectra of TOH adsorbed on Cu (adTOH) and that of polyTOH are compared in Fig. 2S (Supplementary Information). adTOH spectrum shows the distinctive contributions of pure TOH with additional signals attributed to cetonic structures (1640 cm^{-1}) that account for the presence of adTOH on copper surface and the evidence of its oxidation under OCP conditions (a similar spectrum is obtained for adCarv). Interestingly, marked differences between adTOH and polyTOH spectra in the 3000 cm^{-1}–3550 cm^{-1} region can be noticed.

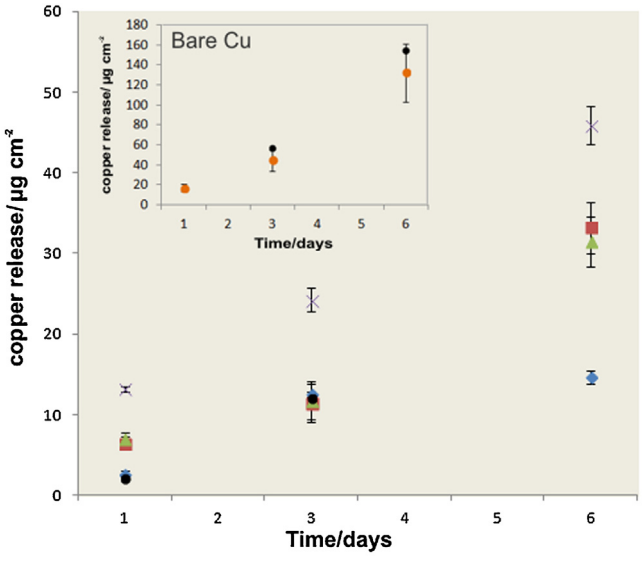

Fig. 6. Copper ion release from treated Cu samples after their immersion for 1, 3 and 6 days in KCl solution (0.136 M) obtained by a colorimetric method (PAN). (■) polyCarvCu 1 cycle; (♦) polyCarvCu 39 cycles; (✕) polyTOHCu 1 cycle; (▲) polyTOHCu 39 cycles. Inset: (●) Copper ion release from bare Cu. Measurements by atomic absorption spectroscopy are also included (•) in the main graph and in the inset. (For interpretation of the references to colour in this figure legend, the reader is referred to the web version of this article.)

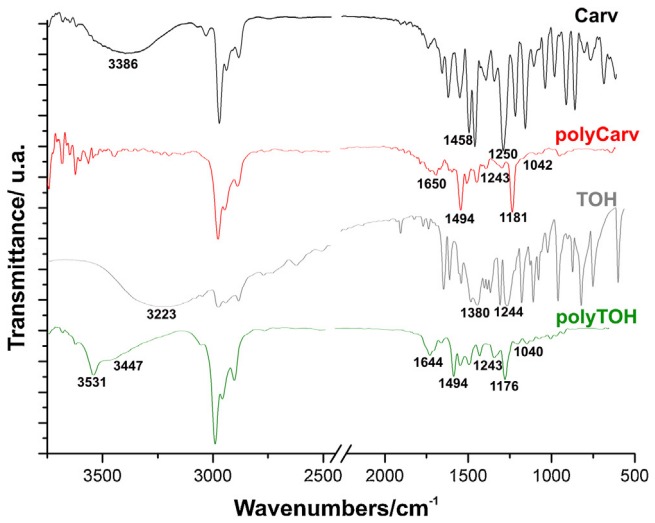

Fig. 7. ATR-FTIR spectra of Carv (pure drug), polyCarvCu, TOH (pure drug) and polyTOHCu. Detail of the polyTOHCu spectrum is shown in Fig. 3S.

PolyTOH and polyCarv spectra formed after cycling in the +0.3 V – +1.0 V potential range are compared in Fig. 7. Peaks at 1494, 1454 and 1176 cm^{-1}, characteristics of polysustituted PC that account for the polymerized state of the layer can be detected. Importantly, the peaks at 1644 cm^{-1} (polyCarv) and 1640 cm^{-1} (polyTOH) indicate the presence of cetonic structures (quinoidal C=O stretch) [19,41,42]. In addition, peaks at 1243, 1494, 1620 and ~1040 cm^{-1} are also detected and can be assigned to ether bonds for phenolic derivatives [19,41,43,44]. Quinoidal and ether bonds denote the oxidation of TOH and Carv during the electropolymerization process.

The spectrum of polyTOHCu shows a signal at 3531 cm^{-1} that is absent in that of polyCarv. This peak is known as hydrogen bond free ν-OH band (HyF/ν-OH) because some authors believe that this OH cannot form H bridges with other molecules such as those of solvent, TOH, etc. [40–42]. Another possibility to explain the presence of HyF/ν-OH is the existence of dimmers, oligomers or quinones structures confined within the polymeric matrix with OH unable to form H bridges [44]. Others authors [37,41,43] reported that this contribution may be assigned to water occluded in the polymeric layer. Additionally, a broad peak at 3447 cm^{-1} was only detected for polyTOHCu (see the detail at higher magnification in supplemental data Fig. 3S) and may be attributed to the OH stretching vibration of hydrogen-bonded O-H···O=C [44].

3.3.2. XPS analysis of polymer coated Cu

The XPS spectra of the Cu2p region for bare Cu, polyCarvCu and polyTOH are shown in Fig. 8. They depict low signals for Cu with electropolymerized layers, probably due to the low capacitance of the polymeric films.

Table 3 shows the surface atomic percentage of C1s, O1s and Cup2p3/2 of each sample and the Auger parameters (AP) calculated for Cu. AP for bare Cu is in agreement with the metallic copper value reported in the NIST database. However, the AP values decrease upon cycling reaching a value close to that of Cu^{1+} present in Cu_2O species. Fig. 8A1 corresponds to the survey spectra of polyCarv and polyTOH films and Fig. 8A2 shows the typical Cu^{2+} shake up satellites, relatively enhanced, at higher binding energies than the characteristic Cu2p3/2-Cu2p1/2 lines. This indicates, by the Auger parameter, the joint presence of Cu^{2+} and Cu^{1+} species. The organic layer obtained on the Cu surface by

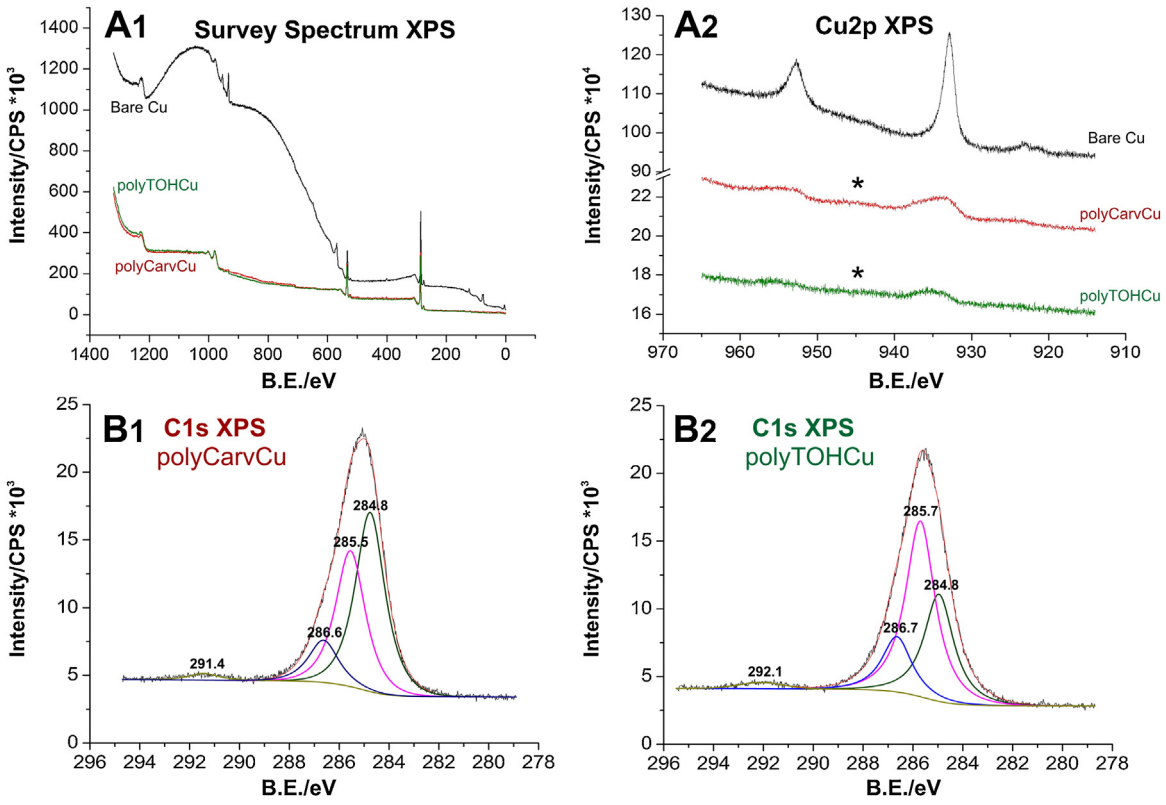

Fig. 8. XPS spectra. A1) Survey XPS spectra of Bare Cu, polyCarvCu and polyTOHCu. A2) Cu2p spectra showing Cu^{2+} shake up satellite (*) B1) C1s spectra for polyCarvCu; B2) C1 s spectra for polyTOHCu.

Table 3
Surface composition obtained by XPS analysis.

	C1 s %	Cu 2p3/2%	O1 s %	C/O	AP Cu	O/Cu
Bare Cu	80,51	5,04	13,01	**6,2**	1851,338	**2,6**
adCarvCu	52,68	10,04	34,10	**1,5**	1850,269	**3,4**
polyCarvCu (1 Cycle)	66,16	0,73	22,58	**2,9**	1847,693	**31,1**
polyCarvCu (5 Cycles)	71,04	0,61	20,15	**3,5**	1847,475	**33,0**
polyCarvCu (39 Cycles)	78,52	0,38	19,35	**4,1**	1846,875	**51,2**
adTOHCu	52,39	9,67	34,77	**1,5**	1849,974	**3,6**
polyTOHCu (1 Cycle)	69,87	0,90	16,73	**4,2**	1848,319	**18,6**
polyTOHCu (5 Cycles)	79,42	0,70	15,31	**5,2**	1847,606	**21,7**
polyTOHCu (39 Cycles)	77,90	0,44	20,29	**3,8**	1846,809	**46,4**

electropolymerization probably attenuates most of the underneath metallic photoelectron signal. Therefore mostly the copper-polymer interface shapes Cu2p signal in both films. The intensity of the signal decreases upon cycling, with lower intensities in case of TOH. The attenuation of the Cu photoelectron signal can be related to the increased thickness of the polymeric layer. Thus, the chemical information of the signal corresponds to a few atomic layers in copper depth.

O1s % for polyCarvCu and polyTOHCu are markedly lower than those of adCarv and adTOH and C1s/O1s relationships are higher for polymerized layers. Initially the higher values correspond to TOH but, unlike Carv, after 39 cycles the relationship decreases mainly due to the increase in the oxygen content.

C1s contributions were mainly fitted with four components (Fig. 8B1, B2): i) 284.8 eV attributed to C-C and C-H; ii) (285.5 eV, 285.7 eV) associated $C_{(ph)}$-O; iii) (291.4 eV, 292.1 eV) due to the π->π^* transition satellite of the aromatic structure [45] for polyCarv and polyTOH, respectively. Considering that (iii), related to aromatic structures) is nearly zero in case of adCarvCu and adTOHCu it could be inferred that there is a higher number of Carv or TOH molecules on Cu surface with polyCarvCu/polyTOHCu than in the case of adCarvCu/adTOHCu. A fourth contribution (iv) (286.8 eV, 286,7 eV, for polyCarv and polyTOH, respectively) could be assigned to C quinone group (C=O) [35,46–48] in agreement with the signal detected by ATR-FTIR analysis.

The evolution of the composition of polyCarv and polyTOH films on Cu substrates during cycling is different for each compound. Thus, contribution (ii) of polyTOH (C(ph)-O) increases upon cycling and this increase is more noticeable than that of polyCarv. Accordingly, after 39 cycles the relative contribution of (ii) to the total C1 s peak is 50% for polyCarvCu and 30% for polyTOHCu, respectively. This can be associated to the way each isomer anchors on copper surface and the grade of susceptibility to form polymeric structures due to steric hindrance, that leads to a higher oxidation, i.e. higher number of O per molecule, in case of polyTOH layer.

3.3.3. AFM imaging

AFM images show (Fig. 9) the surface morphology of polyCarv and polyTOH after the cycling process (39 cycles). A closed packed morphology fully covered the Cu surface and round nanoflakes can be distinguished on the surface. The line profile of the AFM image suggests that these particles may be less than 5 nm high in case of polyCarvCu while globular particles close to 35 nm high that form a cauliflower like structures [49] were distinguished for polyTOH. Roughness parameters included in Fig. 9 confirm the higher roughness of polyTOH layer.

3.4. Electropolymerization mechanism

The proposed mechanism to interpret the complex oxidation processes of Carv and TOH were adapted from those reported by

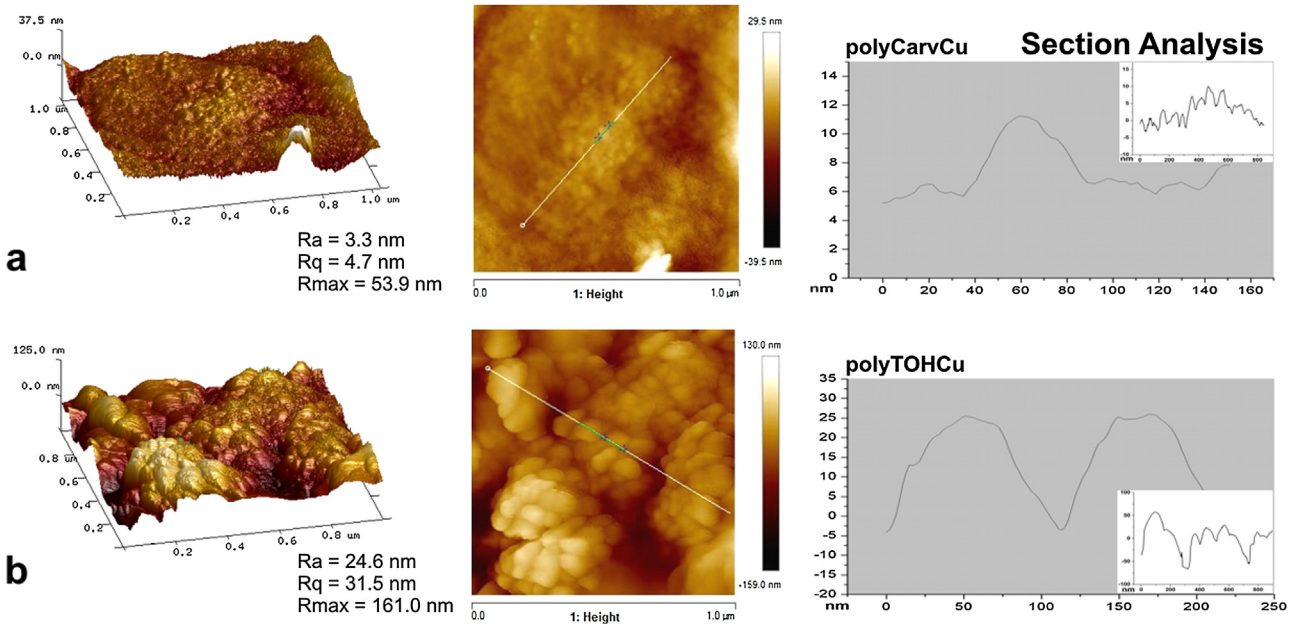

Fig. 9. AFM images corresponding to polyCarvCu (a) and polyTOHCu (b). Section analyses (inset) and details are shown on the left.

Garfias-García et al. [50] and Bao et al. [39] for polypyrrole and polyphenol, respectively, and involve the reactions shown below.

Firstly, and according to ATR-FTIR results (see Fig. 2S), the molecules adsorbed on the metal surface (Reaction (1)). Contribution in the region close to 3300 cm^{-1} absent in the control without Carv/TOH is associated to the adsorbed molecules. These single adsorbed molecules may be oxidized and form adsorbed dimers in one or two steps (Eqs. (2)–(4)):

$$PhD_{(ac)} \leftrightarrow PhD_{(ad)} \quad (1)$$

$$PhD_{(ad)} + PhD_{(ad)} \leftrightarrow PhD_{2(ad)} + 2e^- + 2H^+_{(ac)} \quad (2)$$

$$PhD_{(ad)} \leftrightarrow PhD^{\circ+}_{(ad)} + e^- \quad (3)$$

$$PhD^{\circ+}_{(ad)} + PhD_{(ad)} \leftrightarrow PhD_{2(ad)} + e^- + 2H^+_{(ac)} \quad (4)$$

$$PhD_{2(ad)} \leftrightarrow PhD_{2(ad)}{}^- + H^+ \quad (4a)$$

$$PhD_{2(ad)}{}^- \leftrightarrow PhD_{2(ad)}{}^\circ + e^- \quad (4b)$$

where PhD is the phenolic derivative Carv or TOH. Electrooxidation leads to quinone and ether polymeric structures detected by ATR-FTIR spectra. Alternatively, the dimer may lose a proton because it is favorable in basic media and according to Eq. (4a) formation of $PhD_{2(ad)}{}^-$ anions could take place. Subsequently, during polymerization the lost of one electron occurs (Eq. (4b)) [39].

There should be various kinds of dimers as a result of the carbon–oxygen and carbon–carbon coupling. Some dimers may not form ether bonds and will make the polymer retain a large amount of phenol hydroxyls in the structure [39]. According to ATR-FTIR results these types of dimers seem to be more frequent in case of TOH electropolymerization.

PhD cathions and cathionic dimers that return to the solution or remain at the interface may also be formed:

$$2PhD_{(ac)} \leftrightarrow 2PhD^{\circ+}_{(ac)} + 2e^- \quad (5)$$

$$2PhD^{\circ+}_{(ac)} \leftrightarrow PhD^{2+}{}_{2(ac)} \quad (6)$$

$$PhD^{2+}{}_{2(ac)} \leftrightarrow PhD_{2(ac)} + 2H^+_{(ac)} \quad (7)$$

Thus, successive oxidations may transform dimers in oligomers that return to the solution (Eqs. (8)–(11)) close to the metal or remain adsorbed and may form aggregates on the surface (Eqs. (12) and (13)).

$$PhD_{n(ac)} \leftrightarrow PhD^{\circ+}{}_{n(ac)} + e^- \quad (8)$$

$$PhD_{j(ac)} \leftrightarrow PhD^{\circ+}{}_{j(ac)} + e^- \quad (9)$$

$$PhD^{\circ+}{}_{n(ac)} + PhD^{\circ+}{}_{j(ac)} \leftrightarrow PhD^{2+}{}_{j+n(ac)} \quad (10)$$

$$PhD^{2+}{}_{j+n(ac)} \leftrightarrow PhD_{j+n(s)} + 2H^+_{(ac)} \quad (11)$$

$$PhD_{n(ad)} \leftrightarrow PhD^{\circ+}{}_{n(ad)} + e^- \quad (12)$$

$$PhD^{\circ+}{}_{n(ad)} + PhD_{(ad)} \leftrightarrow PhD_{n+1(s)} + e^- + 2H^+_{(ac)} \quad (13)$$

$$PhD_{m(s)} + PhD_{(ac)} \leftrightarrow PhD_{m+1(s)} + 2e^- + 2H^+_{(ac)} \quad (14)$$

In the Reactions (5)–(11) $PhD_{(ac)}$, represents the monomer species in solution, close to the metal, $PhD^{\circ+}{}_{(ac)}$ a cation radical formed by oxidation of the monomer, $PhD_{(ac)}$; and $PhD_{2(ac)}$ is the

dimer in solution, $PhD_{n(ac)}$ and $PhD_{j(ac)}$ represent different oligomers in solution close to the metal or within the open layer of polyTOH and $PhD_{j+n(s)}$ is an insoluble oligomer.

The electrooxidation process [12–14] in case of Carv leads to the formation of 2D layer that blocks the metal surface. In Reaction (12) $PhD^{\circ+}_{n(ad)}$ is an adsorbed radical cation oligomer resulting from the oxidation of the oligomer $PhD_{n(ad)}$ which further oxidation leads to $PhD_{n+1(s)}$ (Reaction (13)) or to $PhD_{m+1(s)}$ (Reaction (14)).

According to Fig. 1, OH group of TOH is close to the isopropyl group and the formation of an ordered and compact 2D polymeric layer is probably hindered in due to steric impediments. In case of polyphenol it was found that the mayor portion of the coating grows following a flake-like mode (50 nm flakes) that builds layers parallel to the metal with only a minor portion of the polymer that grows in a linear mode, forming sticks [39]. SEM and AFM observations (Figs. 3 and 9) seem to indicate that polyCarv coating mainly grows following a flake-like mode but, unlike polyphenol, the flakes are very small (5 nm height), forming a compact 2D layer. Conversely, the TOH polymerization mostly yields larger flakes (35 nm height) that follows either stick structures that are vertical to the metal plane or cauliflower structures. In view of ATR-FTIR results, more —OH groups may remain unbound on sticks and cauliflower surfaces of polyTOH. This way of growing also leads to the formation of cracks like that shown in Fig. 3 (similar to those of polyphenol [39]) that decreases the protective action of the layer. Thus, polyTOH soft open layer may allow the transport of ions that, according to copper ions measurements, favors the copper corrosion process.

4. Conclusions

TOH and Carv, natural compounds components of some essential oils, adsorb on copper surface and the oxidation of the adsorbed species leads to cetonic structures. However, the electropolymerized layers of these structural isomers are quite different. Results show the high impact of —OH position in the phenolic ring on the electropolymerization process that influence on the appearance, composition, structure and protective characteristics of the polymeric layers.

The analysis of the electrochemical, surface studies, spectroscopic results and copper ions release measurements revealed that different mechanisms are involved in the electropolymerization processes of Carv and TOH.

During potentiodynamic cycles Carv and TOH oxidize on Cu, blocking the surface at different degrees with the oxidation products that were detected by ATR-FTIR and XPS analysis. These oxidation products include quinoidal and ether bonds that hinder the access to the active sites of the metal surface. However, ATR-FTIR results for polyTOH show peaks at 3530 and 3450 cm^{-1}, absent in case of polyCarv, attributed to hydrogen free ν-OH or water confined within the polymeric matrix. Different C1s/O1s relationships were also found by XPS for polyCarv and polyTOH layers. Deconvolution of C1s signal of XPS spectra leads to four contributions with different proportions for polyCarv and polyTOH.

The polyCarv layer formed after several potentiodynamic cycles is transparent and shows high protection against corrosion while that of polyTOH is brownish and weakly protective. TOH polymerization mostly yields larger flakes (35 nm height) than those of polyCarv (5 nm height) and leads to either cauliflower structures or to stick structures that are vertical to the metal plane where cracks are found. Thus, copper ions release by polyTOH in chloride solutions was markedly higher than that of polyCarv.

Results are important in relation to the selection of the species of the aromatic plants that will be the best sources of the essential oils to be used as ecofriendly corrosion inhibitors. Thus, according to electrochemical data, *Origanum vulgare*, very reach in Carv, should be a better source than *Origanum X applii* and *Thymus vulgaris* whose main component is TOH.

Acknowlegments

The authors also acknowledge the sponsorship of CONICET, UNLP (11/I221), ANPCyT (PICT 2012-1795) and PPL (2011 0003). Author wish to acknowledge to Dr. Natalia Fagali and E. Llerena Sutter for their assistance in the colorimetric measurements of copper ions.

Appendix A. Supplementary data

Supplementary data associated with this article can be found, in the online version, at http://dx.doi.org/10.1016/j.electacta.2016.08.100.

References

[1] R.E. Melchers, Bi-modal trends in the long-term corrosion of copper and high copper alloys, Corros. Sci. 95 (2015) 51–61, doi:http://dx.doi.org/10.1016/j.corsci.2015.02.001.
[2] A. Drach, I. Tsukrov, J. DeCew, J. Aufrecht, A. Grohbauer, U. Hofmann, Field studies of corrosion behaviour of copper alloys in natural seawater, Corros. Sci. 76 (2013) 453–464, doi:http://dx.doi.org/10.1016/j.corsci.2013.07.019.
[3] X. Zhang, I.O. Wallinder, C. Leygraf, Mechanistic studies of corrosion product flaking on copper and copper-based alloys in marine environments, Corros. Sci. 85 (2014) 15–25, doi:http://dx.doi.org/10.1016/j.corsci.2014.03.028.
[4] G. Kear, B.D. Barker, F.C. Walsh, Electrochemical corrosion of unalloyed copper in chloride media —-a critical review, Corros. Sci. 46 (2004) 109–135, doi:http://dx.doi.org/10.1016/s0010-938x(02)00257-3.
[5] I. Vopálenská, L. Váchová, Z. Palková, New biosensor for detection of copper ions in water based on immobilized genetically modified yeast cells, Biosens. Bioelectron. 72 (2015) 160–167, doi:http://dx.doi.org/10.1016/j.bios.2015.05.006.
[6] D.A. Shifler, Understanding material interactions in marine environments to promote extended structural life, Corros. Sci. 47 (2005) 2335–2352, doi:http://dx.doi.org/10.1016/j.corsci.2004.09.027.
[7] Y.C. Pan, Y. Wen, R. Zhang, Y.Y. Wang, Z.R. Zhang, H.F. Yang, Electrochemical and SERS spectroscopic investigations of 4-methyl-4H-1,2,4-triazole-3-thiol monolayers self-assembled on copper surface, Appl. Surf. Sci. 258 (2012) 3956–3961, doi:http://dx.doi.org/10.1016/j.apsusc.2011.12.070.
[8] Sudheer, M.A. Quraishi, Electrochemical and theoretical investigation of triazole derivatives on corrosion inhibition behavior of copper in hydrochloric acid medium, Corros. Sci. 70 (2013) 161–169, doi:http://dx.doi.org/10.1016/j.corsci.2013.01.025.
[9] S.M. Milić, M.M. Antonijević, Some aspects of copper corrosion in presence of benzotriazole and chloride ions, Corros. Sci. 51 (2009) 28–34, doi:http://dx.doi.org/10.1016/j.corsci.2008.10.007.
[10] H. Tian, Y.F. Cheng, W. Li, B. Hou, Triazolyl-acylhydrazone derivatives as novel inhibitors for copper corrosion in chloride solutions, Corros. Sci. 100 (2015) 341–352, doi:http://dx.doi.org/10.1016/j.corsci.2015.08.022.
[11] Z. Khiati, A.A. Othman, M. Sanchez-Moreno, M.C. Bernard, S. Joiret, E.M.M. Sutter, V. Vivier, Corrosion inhibition of copper in neutral chloride media by a novel derivative of 1 2,4-triazole, Corros. Sci. 53 (2011) 3092–3099, doi:http://dx.doi.org/10.1016/j.corsci.2011.05.042.
[12] G. Moretti, F. Guidi, G. Grion, Tryptamine as a green iron corrosion inhibitor in 0.5 M deaerated sulphuric acid, Corros. Sci. 46 (2004) 387–403, doi:http://dx.doi.org/10.1016/S0010-938X(03)00150-1.
[13] A.Y. El-Etre, M. Abdallah, Z.E. El-Tantawy, Corrosion inhibition of some metals using lawsonia extract, Corros. Sci. 47 (2005) 385–395, doi:http://dx.doi.org/10.1016/j.corsci.2004.06.006.
[14] E.E. Oguzie, A.I. Onuchukwu, P.C. Okafor, E.E. Ebenso, Corrosion inhibition and adsorption behaviour of Ocimum basilicum extract on aluminium, Pigment Resin Technol. 35 (2006) 63–70, doi:http://dx.doi.org/10.1108/03699420610652340.
[15] A.M. Abdel-Gaber, E. Khamis, H. Abo-ElDahab, S. Adeel, Inhibition of aluminium corrosion in alkaline solutions using natural compound, Mater. Chem. Phys. 109 (2008) 297–305, doi:http://dx.doi.org/10.1016/j.matchemphys.2007.11.038.
[16] E. Khamis, N. Alandis, Herbs as New Type of Green Inhibitors For Acidic Corrosion of Steel, Materwiss. Werkst. 33 (2002) 550–554, doi:http://dx.doi.org/10.1002/1521-4052(200209)33:9<550::AID-MAWESSO>3.0.CO;2-G.
[17] A.S. Fouda, K. Shalabi, A.A. Idress, Thymus Vulgarise Extract as Nontoxic Corrosion Inhibitor for Copper and α −Brass in 1 M HNO 3 Solutions, Int. J. Electrochem. Sci. 9 (2014) 5126–5154.
[18] S. Umoren, Z.M. Gasem, I.B. Obot, Natural products for material protection: Inhibition of mild steel corrosion by date palm seed extracts in acidic media,

Ind. Eng. Chem. Res. 52 (2013) 14855–14865, doi:http://dx.doi.org/10.1021/ie401737u.
[19] M. Ferreira, H. Varela, R.M. Torresi, G. Tremiliosi-Filho, Electrode passivation caused by polymerization of different phenolic compounds, Electrochim. Acta. 52 (2006) 434–442, doi:http://dx.doi.org/10.1016/j.electacta.2006.05.025.
[20] L.G. Andión, P. Garcéz, R. Lapuente, J.L. Vázquez, F. Cases, P. Garcés, et al., Corrosion behaviour at the interface of steel bars embedded in cement slurries Effect of phenol polymer coatings, Corros. Sci. 44 (2002) 2805–2816, doi:http://dx.doi.org/10.1016/S0010-938X(02)00077-X.
[21] M. Bertuola, C.A. Grillo, M.A. Fernández Lorenzo, Reduction of copper ions release by a novel ecofriendly electropolymerized nanolayer obtained from a natural compound (carvacrol), J. Hazard. Mater. 313 (2016) 262–271, doi:http://dx.doi.org/10.1016/j.jhazmat.2016.03.086.
[22] T.A. Enache, A.M. Oliveira-Brett, Phenol and para-substituted phenols electrochemical oxidation pathways, J. Electroanal. Chem. 655 (2011) 9–16, doi:http://dx.doi.org/10.1016/j.jelechem.2011.02.022.
[23] E. De Falco, E. Mancini, G. Roscigno, E. Mignola, O. Taglialatela-Scafati, F. Senatore, Chemical composition and biological activity of essential oils of origanum vulgare L. subsp. vulgare L. under different growth conditions, Molecules. 18 (2013) 14948–14960, doi:http://dx.doi.org/10.3390/molecules181214948.
[24] P.E. Pensel, M.A. Maggiore, L.B. Gende, M.J. Eguaras, M.G. Denegri, M.C. Elissondo, Efficacy of Essential Oils of Thymus vulgaris and Origanum vulgare on Echinococcus granulosus, Interdiscip Perspect Infect Dis 2014 (2014).
[25] J.S. Dambolena, M.P. Zunino, E.I. Lucini, R. Olmedo, E. Banchio, P.J. Bima, J.A. Zygadlo, Total phenolic content, radical scavenging properties, and essential oil composition of Origanum species from different populations, J. Agric. Food Chem. 58 (2010) 1115–1120, doi:http://dx.doi.org/10.1021/jf903203n.
[26] A. Guenbour, A. Kacemi, A. Benbachir, L. Aries, Electropolymerization of 2-aminophenol. Electrochemical and spectroscopic studies, Prog. Org. Coatings. 38 (2000) 121–126, doi:http://dx.doi.org/10.1016/S0300-9440(00)00085-0.
[27] A. Guenbour, A. Kacemi, A. Benbachir, Corrosion protection of copper by polyaminophenol films, Prog. Org. Coatings. 39 (2000) 151–155, doi:http://dx.doi.org/10.1016/S0300-9440(00)00141-7.
[28] G. Mengoli, M.M. Musiani, An Overview of Phenol Electropolymerization for Metal Protection, J. Electrochem. Soc. 134 (1987) 643C–652C, doi:http://dx.doi.org/10.1149/1.2100379.
[29] M.J. Ahmed, M. Saifuddin, T. Jannat, S.C. Bhattacharjee, A Rapid Spectrophotometric Method for the Determination of Copper in Real, Environmeental Biological and Soil Samples Using 1-(2-pyridylazo)-2-naphthol, Green Chem. 4 (2010) 1–12.
[30] H.-H. Strehblow, V. Maurice, P. Marcus, Initial and later stages of anodic oxide formation on Cu, chemical aspects, structure and electronic properties, Electrochim, Acta. 46 (2001) 3755–3766, doi:http://dx.doi.org/10.1016/S0013-4686(01)00657-0.
[31] J. Kunze, V. Maurice, L.H. Klein, H.-H. Strehblow, P. Marcus, In Situ Scanning Tunneling Microscopy Study of the Anodic Oxidation of Cu(111) in 0.1 M NaOH, J. Phys. Chem. B. 105 (2001) 4263–4269, doi:http://dx.doi.org/10.1021/jp004012i.
[32] M.R. Othman, J. Salimon, Analysis of Ethanol Using Copper and Nickel Sheet, Malaysian, J. Anal. Sci. 11 (2007) 379–387.
[33] W. Novakowski, M. Bertotti, T.R.L.C. Paixão, Use of copper and gold electrodes as sensitive elements for fabrication of an electronic tongue: Discrimination of wines and whiskies, Microchem. J. 99 (2011) 145–151, doi:http://dx.doi.org/10.1016/j.microc.2011.04.012.
[34] T.R.L.C. Paixão, D. Corbo, M. Bertotti, Amperometric determination of ethanol in beverages at copper electrodes in alkaline medium, Anal. Chim. Acta. 472 (2002) 123–131, doi:http://dx.doi.org/10.1016/S0003-2670(02)00942-X.
[35] P. Krawczyk, J.M. Skowroński, Multiple anodic regeneration of exfoliated graphite electrodes spent in the process of phenol electrooxidation, J. Solid State Electrochem. 18 (2014) 917–928, doi:http://dx.doi.org/10.1007/s10008-013-2335-5.
[36] S. Sundaram, S.K. Annamalai, Selective immobilization of hydroquinone on carbon nanotube modified electrode via phenol electro-oxidation method and its hydrazine electro-catalysis and Escherichia coli antibacterial activity, Electrochim. Acta. 62 (2012) 207–217, doi:http://dx.doi.org/10.1016/j.electacta.2011.12.044.
[37] X. Yang, J. Kirsch, J. Fergus, A. Simonian, Modeling analysis of electrode fouling during electrolysis of phenolic compounds, Electrochim. Acta. 94 (2013) 259–268, doi:http://dx.doi.org/10.1016/j.electacta.2013.01.019.
[38] Y. Zhang, Q. Li, H. Cui, J. Zhai, Removal of phenols from the aqueous solutions based on their electrochemical polymerization on the polyaniline electrode, Electrochim. Acta. 55 (2010) 7219–7224, doi:http://dx.doi.org/10.1016/j.electacta.2010.07.002.
[39] J. Wang, M. Jiang, F. Lu, Electrochemical quartz crystal microbalance investigation of surface fouling due to phenol oxidation, J. Electroanal. Chem. 444 (1998) 127–132.
[40] I.S. Al-Sheibany, Qualitative and Quantitative Evaluation of some Organic Compounds in Iraqi Thyme, Natl. J. Chem. 19 (2005) 366–379.
[41] M. Gattrell, D.W. Kirk, A Fourier Transform Infrared Spectroscopy Study of the Passive Film Produced During Aqueous Acidic Phenol Electro- Oxidation, J Electrochem Soc. 139 (1992) 2736–2744, doi:http://dx.doi.org/10.1149/1.2068972.
[42] A. Ciszewski, G. Milczarek, Preparation and general properties of chemically modified electrodes based on electro synthesized thin polymeric films derived from eugenol, Electroanalysis 13 (2001) 860–867 Go to ISI>//000170124700009.
[43] Sadtler Research Laboratories, W.W., Simons, S.R., Laboratories. The Sadtler handbook of infrared spectra, Philadelphia, Sadtler Research Laboratories, Philadelphia, 1978.
[44] L. Bao, R. Xiong, G. Wei, Electrochemical polymerization of phenol on 304 stainless steel anodes and subsequent coating structure analysis, Electrochim. Acta. 55 (2010) 4030–4038, doi:http://dx.doi.org/10.1016/j.electacta.2010.02.052.
[45] D. Briggs, Surface analysis of polymers by XPS and static SIMS, Cambridge University Press, Cambridge, 1998, doi:http://dx.doi.org/10.1017/CBO9781107415324.004.
[46] J.L. Solomon, R.J. Madix, J. Stöhr, Orientation and absolute coverage of benzene, aniline, and phenol on Ag(110) determined by NEXAFS and XPS, Surf. Sci. 255 (1991) 12–30, doi:http://dx.doi.org/10.1016/0039-6028(91)90008-G.
[47] Z.R. Yue, W. Jiang, L. Wang, S. Gardner, C.U. Pittman Jr., Surface characterization of electrochemically oxidized carbon fibers, Carbon 37 (1999) 1797–1807, doi:http://dx.doi.org/10.1016/S0008-6223(99)00048-2.
[48] M. Gattrell, D.W. Kirk, A Study of Electrode Passivation during Aqueous Phenol Electrolysis, J. Electrochem. Soc. 140 (1993) 903, doi:http://dx.doi.org/10.1149/1.2056225.
[49] J.I. Martins, M. Bazzaoui, T.C. Reis, S.C. Costa, M.C. Nunes, L. Martins, et al., The effect of pH on the pyrrole electropolymerization on iron in malate aqueous solutions, Prog. Org. Coatings. 65 (2009) 62–70, doi:http://dx.doi.org/10.1016/j.porgcoat.2008.09.011.
[50] E. Garfias-García, M. Romero-Romo, M.T. Ramírez-Silva, J. Morales, M. Palomar-Pardavé, Mechanism and kinetics of the electrochemical formation of polypyrrole under forced convection conditions, J. Electroanal. Chem. 613 (2008) 67–79, doi:http://dx.doi.org/10.1016/j.jelechem.2007.10.013.